changes occurring in $CaAl_4$ after martensitic transformation at 130 °C. With this distortion, [89Bru] indexed all of the reflections of the powder pattern of $CaGa_4$. For structural analysis, a single crystal was extracted from an 84.6 at.% Ga alloy. Then, 293 reflections were used to refine the structure with $R = 0.057$. The parameters of the monoclinic lattice were found as $a = 0.6181$ (1), $b = 0.6130$ (1), $c = 0.6117$ (2) nm, and $\beta = 118.94$ (2)°.

Cited References

*43Lav: F. Laves, "Crystal Structure of $CaGa_2$, $LaGa_2$, and $CeGa_2$," *Naturwissenschaften., 31.*, 145 (1943) in German. (Equi Diagram, Crys Structure; Experimental)

52Eva: R.M. Evance and R.I. Jaffe, "Low Melting Gallium Alloys," *Trans. AIME, 194,* 153-156 (1952). (Equi Diagram; Experimental)

*65Bru: G. Bruzzone, "MX_4 Compounds of Alkaline Earth Metals with IIIB Group Elements," *Acta Crystallogr., 18,* 1081-1082 (1965). (Equi Diagram, Crys Structure; Experimental)

*66Bru: G. Bruzzone, "Binary Systems Ca-Ga, Sr-Ga, Ba-Ga," *Boll. Sci. Fac. Chim. Industr. Bologna, 24,* 113-132 (1966) in Italian. (Equi Diagram, Crys Structure; Experimental; #)

66Kri: P.I. Kripyakevich, E.I. Gladyshevskii, and D.I. Dzyana, "Binary Intermetallic Compounds of the $BaAl_4$ Type Containing Gallium," *Sov. Phys. Crystallogr., 10,* 392-394 (1966). (Equi Diagram, Crys Structure; Experimental)

70Bru: G. Bruzzone, "Some Intermetallic Compounds MX_2 Formed by Ca, Sr and Ba," *Atti Acad. Nat. Lincei, Rend. Sc. Fis. Mat. Nat., 48,* 235-241 (1970) in Italian. (Equi Diagram, Crys Structure; Experimental)

*78Bru: G. Bruzzone, E. Francheschi, and F. Merlo, "M_5X_3 Intermediate Equis Formed by Ca, Sr and Ba," *J. Less-Common Met., 60,* 59-63 (1978). (Equi Diagram, Crys Structure; Experimental)

*79Pal: A. Palenzona and S. Cirafici, "The Ytterbium-Gallium System," *J. Less-Common Met., 63,* 105-109 (1979). (Equi Diagram, Crys Structure; Experimental)

85Cha: M.W. Chase, Jr., C.A. Davies, J.R. Downey, Jr., D.J. Frurip, R.A. McDonald, and A.N. Syverud, "JANAF Thermochemical Tables," 3rd ed., *J. Phys. Chem. Ref. Data, 14* (Suppl. 1), part 1, 685-688 (1985). (Equi Diagram, Thermo; Compilation)

85Kim: S.G. Kim, Yu.M. Grin', E.I. Gladyshevskii, "Equi Equilibria in the System Ca-Ga-Fe at 670 K," *Dop. Akad. Nauk Ukr. RSR A, Fiz.-Mat., Tekh., 1,* 76-78 (1985) in Ukrainian. (Equi Diagram; Crys Structure; Experimental)

85Yat: S.P. Yatsenko, O.M. Sichevich, Ya.P. Yarmolyuk, and Yu.M. Grin', "The Crystal Structure of the Eu_3Ga_8 Compound," *Dop. Akad. Nauk. Ukr. RSR B, Geol., Khim., Biol., 7,* 55-57 (1985) in Russian. (Equi Diagram, Crys Structure; Experimental)

*86Cor: G. Cordier, H. Schafer, and M. Stelter, "Electron Deficient Compounds of Gallium: Crystal Structure of Ca_3Ga_5," *Z. Anorg. Allg. Chem., 539,* 33-38 (1986) in German. (Equi Diagram, Crys Structure; Experimental)

*86For: M.L. Fornasini and M. Pani, "$Ca_{28}Ga_{11}$, a Structure with Three Types of Coordination Polyhedra around the Gallium Atoms," *Acta Crystallogr., C, 42,* 394-396 (1986). (Equi Diagram, Crys Structure; Experimental)

*86Mer: F. Merlo and M.L. Fornasini, "The Pseudobinary Systems $SrAg_{1-x}Zn_x$, $CaCu_{1-x}Ga_x$ and $CaCu_{1-x}Ge_x$ and their Use for Testing Structural Maps," *J. Less-Common Met., 119,* 45-61 (1986). (Equi Diagram, Crys Structure; Experimental)

*89Bru: G. Bruzzone, M.L. Fornasini, and F. Merlo, "Re-examination of the Ca-Ga System and Crystal Structure of $CaGa_4$, a Monoclinic Distortion of the $BaAl_4$-Type," *J. Less-Common Met., 154,* 67-77 (1989). (Equi Diagram, Crys Structure; Experimental; #)

*89For: M.L. Fornasini and F. Merlo, "The Crystal Structure of $Ca_{11}Ga_7$," *Z. Kristallogr., 187,* 111-115 (1989). (Equi Diagram, Crys Structure; Experimental)

*Indicates key paper.

#Indicates presence of a phase diagram.

Ca-Ga evaluation contributed by **V.P. Itkin**, Department of Metallurgy and Materials Science, University of Toronto, Toronto, Ontario M5S 1A4, Canada and **C.B. Alcock**, Center for Sensor Materials, University of Notre Dame, 114 Cushing Hall, Notre Dame, IN 46556. This work was supported by a grant from ASM International. Literature searched through 1990. Part of the bibliographic search was provided by ASM International. Professor Alcock and Dr. Itkin are the Alloy Phase Diagram Program Category Editors for binary alkaline earth alloys.

The Al-Zr (Aluminum-Zirconium) System

By J. Murray
Alcoa Technical Center
and
A. Peruzzi and J.P. Abriata
Centro Atómico Bariloche

Equilibrium Diagram

The assessed Zr-Al phase diagram (Fig. 1) is based primarily on the work of [39Fin], [54Mcp], [60Eds], [62Eds], [62Pot], [83Sch], and [84Kem], and includes: (1) the liquid, L; (2) the bcc terminal solution, (βZr), in which Al has a maximum solubility of 26 at.% at 1350 °C; (3) the cph terminal solid solution, (αZr), which shows a maximum solubility of 10.5 at.% Al at 940 °C; (4) the intermediate compound Zr_3Al with the cubic $AuCu_3$-type structure, stable up to the peritectic temperature of 988 °C; (5) the hexagonal $InNi_2$-type intermediate compound Zr_2Al, stable up to the peritectic temperature of 1250 °C; (6) the tetragonal compound Zr_5Al_3, isostructural with Si_3W_5, stable in the temperature range from ~1000 to 1400 °C where it decomposes peritectically; (7) the tetragonal compound Zr_3Al_2 stable up to the peritectic temperature of 1480 °C; (8) the hexagonal compound Zr_4Al_3, stable up to the peritectoid temperature of ~1030 °C; (9) the

hexagonal Ga_4Ti_5-type intermediate compound Zr_5Al_4, stable from ~1000 °C to 1550 °C where it melts congruently; (10) the intermediate compound ZrAl with the orthorhombic BCr-type structure, stable up to the peritectoid temperature of 1275 °C; (11) the orthorhombic compound Zr_2Al_3, which decomposes peritectically at 1590 °C; (12) the hexagonal $MgZn_2$-type intermediate compound $ZrAl_2$, stable up to the congruent melting temperature of 1660 °C; (13) the tetragonal compound $ZrAl_3$, which melts congruently at 1580 °C; (14) the fcc terminal solid solution, (Al), with a maximum solubility of 0.083 at.% Zr at its peritectic temperature of 660.8 °C.

Homogeneity ranges are quite restricted for all of the intermediate phases, and their actual compositions correspond closely to those

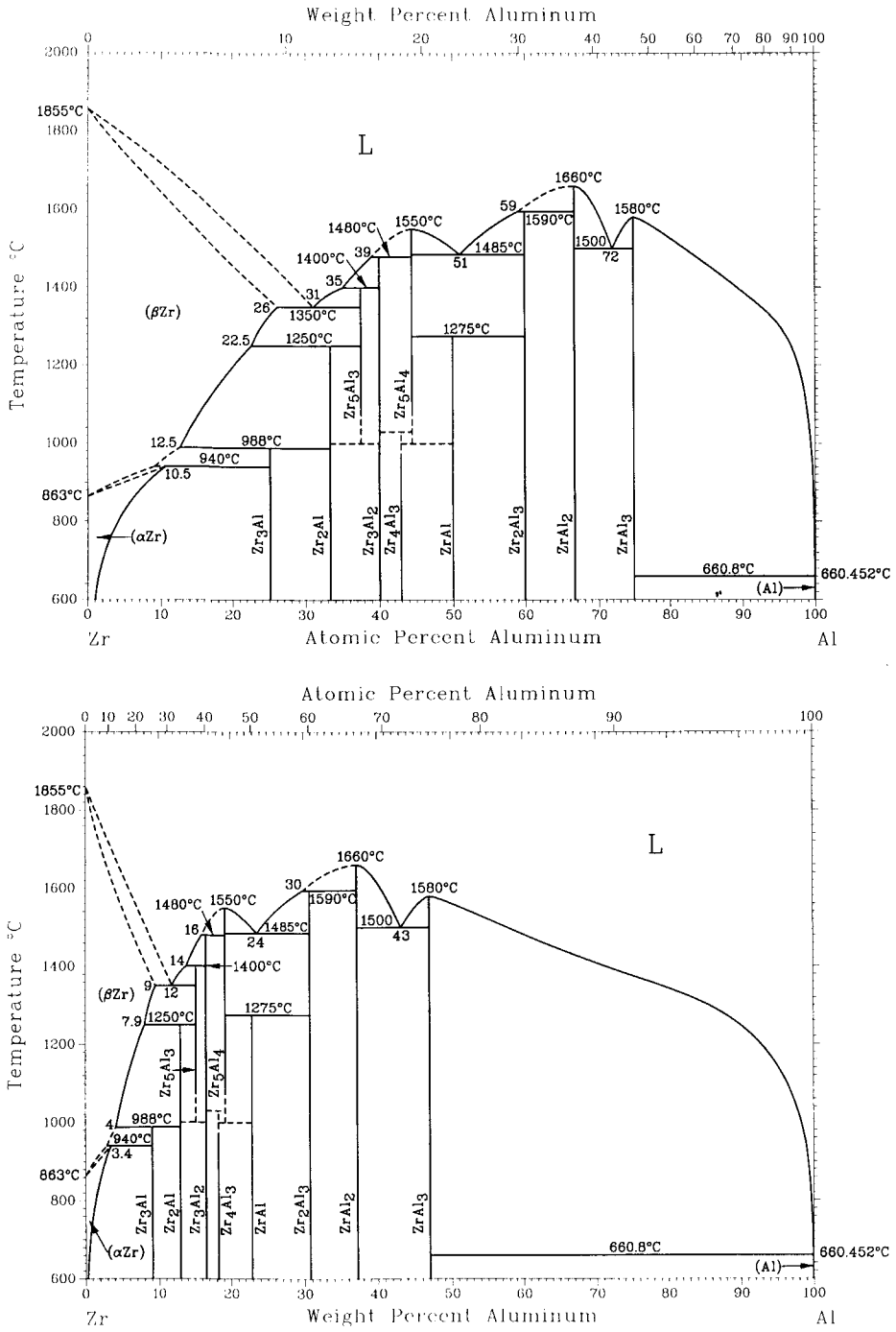

Fig. 1 Assessed Zr-Al phase diagram.

indicated by their respective chemical formulas [54Mcp, 62Pot, 84Kem]. Table 1 summarizes the three-phase equilibria and congruent transformations in the Zr-Al system.

Figure 1 differs from [Massalski1] mainly in some details of the intermediate phases in the range 35 to 45 at.% Al. The melting points of elemental Al and Zr are accepted from [Massalski1] as 660.452 °C and 1855 °C, respectively. The temperature 863 °C for the α ↔ β equilibrium in pure Zr was also adopted from [Massalski1].

Zr-Rich Alloys

The addition of Al stabilizes (αZr) relative to (βZr). The solubility of Al in (αZr) was studied by [54Mcp] (metallography) and [70Tiw] (lattice parameters). The results of these authors are plotted in Fig. 2. The results of [54Mcp] and [70Tiw] agree around 850 °C. However, below this temperature, [70Tiw] found that Al is significantly more soluble in (αZr) than indicated by [54Mcp] (see Fig. 2). The reasons for this discrepancy are not clear. Nevertheless, since we estimate that the contamination levels with interstitial impurities in the samples of [70Tiw] are lower than those of [54Mcp] samples, we accept the results of [70Tiw] in Fig. 1. [76Kub] made the same choice when assessing the Zr-Al system. The (αZr)/[(αZr) + Zr_3Al] boundary (see Fig. 1 and 2) can be described by the semi-empirical expression:

$$\ln[X_{Al}(1-X_{Al})^3] = 1.8888 - 5428.7\,T^{-1}$$

where T is in kelvin and X_{Al} indicates mole fraction. The values we adopt for the temperature of the peritectoid reaction (βZr) + Zr_3Al ↔ (αZr), 940 ± 10 K, and the composition of (αZr) at this reaction, 10.5 ± 0.5 at.% Al, agree with [54Mcp].

No experimental information exists concerning the shape of the two-phase (α + β) field except for some results presented by [54Mcp]. However, these results are particularly affected by contamination as demonstrated by the width of the α ↔ β transition (~20 °C) observed by [54Mcp] even in the case of their pure Zr metal. The experimental data of [54Mcp] are plotted in Fig. 2 as superimposed on the tentative (α + β) boundaries indicated in Fig. 1. These boundaries were drawn primarily to be consistent with the assessed temperature and (αZr) composition at the peritectoid reaction (βZr) + Zr_3Al ↔ (αZr) as well as with the van't Hoff relation with the value 3888 J/mol for the latent heat of the α ↔ β transformation in pure Zr [76Alc]. Hence, the composition obtained for (βZr) at the peritectoid reaction is 8.1 at.% Al.

The (βZr)/[(βZr) + Zr_3Al], (βZr)/[(βZr)+ Zr_2Al] and (βZr)/[(βZr) + Zr_5Al_3] boundaries were investigated by [54Mcp] (metallography). Results from these authors are plotted in Fig. 2 as superimposed on the boundaries given in Fig. 1. The assessed (βZr)/[(βZr) + Zr_2Al] boundary can be described by the semi-empirical expression:

$$\ln[X_{Al}(1-X_{Al})^2] = -0.3433 - 2526\,T^{-1}$$

where T is in kelvin and X_{Al} is again the mole fraction. The solubility of Al in (βZr) at the eutectic reaction L ↔ (βZr) + Zr_5Al_3 was estimated by [54Mcp] to be approximately 26 at.%. The (βZr)/[(βZr) + Zr_2Al] and (βZr)/[(βZr) + Zr_5Al_3] boundaries were also investigated by [75Sch] (metallography) using commercial Zr-Al alloys, and their results are inconsistent with those of [54Mcp].

Because experimental results are not available, the shape of the (βZr) + L two-phase region shown in Fig. 1 is merely tentative; however, it satisfies the van't Hoff relation when the value 18 814 J/mol is used for the latent heat of melting of pure Zr [76Alc].

The existence of the eutectic reaction L ↔ (βZr) + Zr_5Al_3 was established by [54Mcp] who, from thermal analysis and incipient melting, determined its temperature to be 1350 ± 10 °C. From metallographic examination of as-cast alloys, the same authors proposed that the composition of the L phase at this eutectic reaction should be ~29.5 at.% Al. However, from the eutectic

Table 1 Special Points of the Assessed Zr-Al Phase Diagram

Reaction	Composition of the respective phases, at.% Al			Temperature, °C	Reaction type
L ↔ βZr		0		1855	Melting
(βZr) ↔ (αZr)		0		863	Allotropic
L ↔ (βZr) + Zr_5Al_3	31	26	37.5	1350	Eutectic
(βZr) + Zr_5Al_3 ↔ Zr_2Al	22.5	37.5	33.3	1250	Peritectoid
(βZr) + Zr_2Al ↔ Zr_3Al	12.5	33.3	25	988	Peritectoid
(βZr) + Zr_3Al ↔ (αZr)	~8.1	25	10.5	940	Peritectoid
L + Zr_3Al_2 ↔ Zr_5Al_3	~35	40	37.5	1400	Peritectic
Zr_5Al_3 ↔ Zr_2Al + Zr_3Al_2	37.5	33.3	40	~1000	Eutectoid
L + Zr_5Al_4 ↔ Zr_3Al_2	~39	44.4	40	1480	Peritectic
Zr_3Al_2 + Zr_5Al_4 ↔ Zr_4Al_3	40	44.4	42.9	~1030	Peritectoid
Zr_5Al_4 ↔ Zr_4Al_3 + ZrAl	44.4	42.9	50	~1000	Eutectoid
L ↔ Zr_5Al_4		44.4		1550	Congruent
L ↔ Zr_5Al_4 + Zr_2Al_3	~51	44.4	60	1485	Eutectic
Zr_5Al_4 + Zr_2Al_3 ↔ ZrAl	44.4	60	50	1275	Peritectoid
L + $ZrAl_2$ ↔ Zr_2Al_3	~59	66.7	60	1590	Peritectic
L ↔ $ZrAl_2$		66.7		1660	Congruent
L ↔ $ZrAl_2$ + $ZrAl_3$	73.5	66.7	75	1500	Eutectic
L ↔ $ZrAl_3$		75		1580	Congruent
$ZrAl_3$ + L ↔ (Al)	75	99.97	99.92	660.8	Peritectic
L ↔ Al		100		660.452	Melting

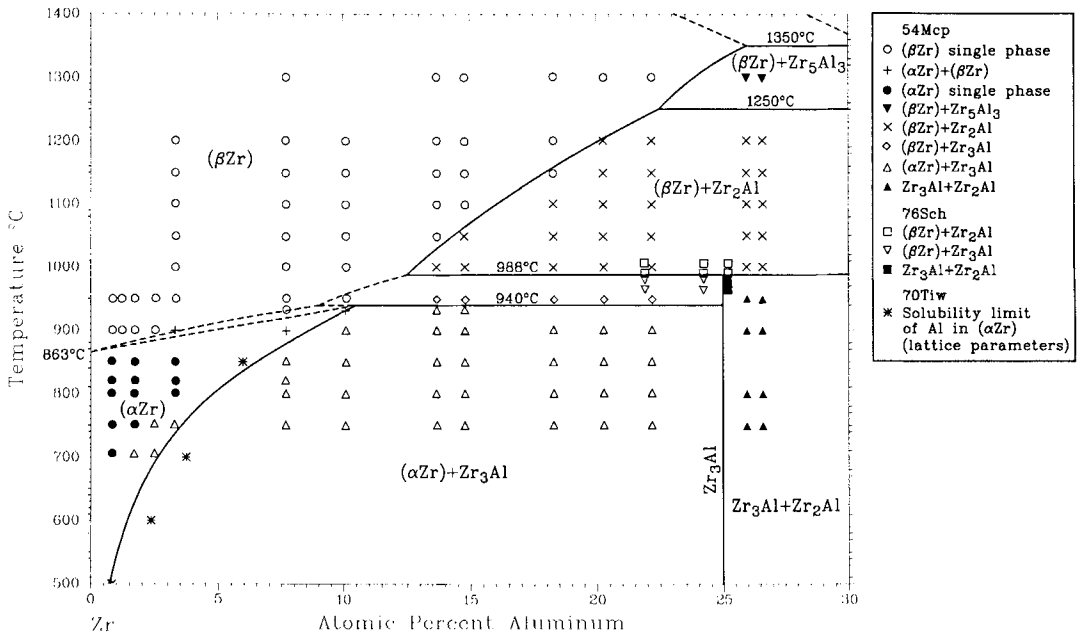

Fig. 2 Zr-rich experimental data superimposed on the corresponding boundary lines shown in Fig. 1.

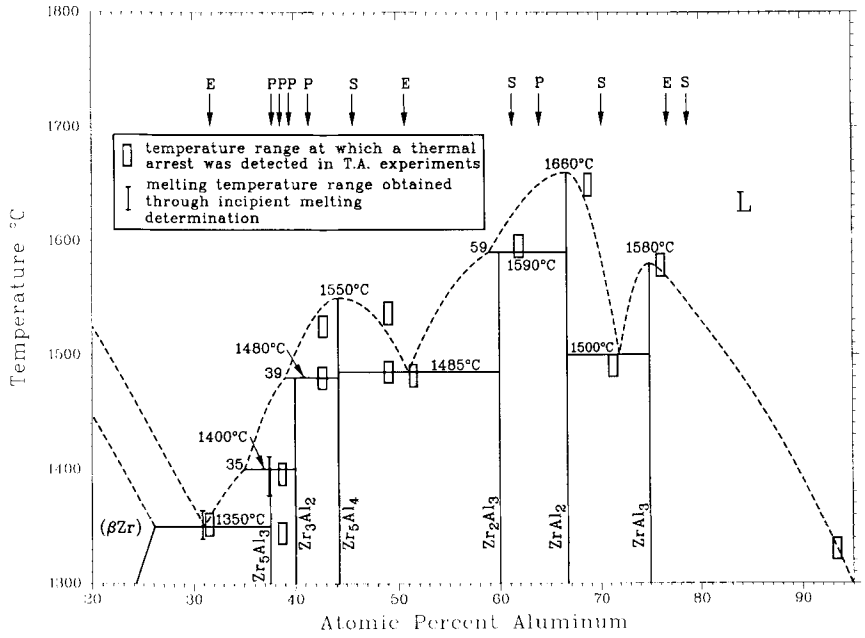

Fig. 3 Assessed Zr-Al liquidus boundary compared to the experimental data by [54Mcp]. E= eutectic, P = Peritectic, and S = single phase, *i.e.,* the as-cast microstructure at the corresponding composition.

microstructure and the single thermal arrest reported by [54Mcp] for alloys with compositions 30.7 and 31.4 at.% Al, respectively, we adopt t he value 31 at.% Al for t his eutectic composition (see Fig. 3).

Intermediate Phases

Zr_3Al

The existence of this compound, which is the Zr-richest intermediate phase of the Zr-Al system, was reported by [54Mcp] and confirmed by several investigators [62Pot, 76Sch, 80Sch]. [55Kee] determined the structure of Zr_3Al to be of the cubic $CuAu_3$-type; this result was corroborated by [62Pot].

Consistent with the observations of [54Mcp] (metallography) and [76Sch] (metallography, microhardness), the temperature of the peritectoid reaction (βZr) + Zr_2Al ↔ Zr_3Al is assessed to be 988 ± 12 °C (see Fig. 2). For the composition of (βZr) at this reaction, we adopt the value 12.5 at.% Al from the numerical expression given above for the (βZr)/[(βZr) + Zr_2Al] boundary.

Zr_2Al

The existence of this phase was reported by [54Mcp] (metallography) who also estimated the temperature of the peritectoid reaction (βZr) + Zr_5Al_3 ↔ Zr_2Al to be within the limits 1200 to 1300 °C (see Fig. 2); the value adopted in Fig. 1 is 1250 ± 40 °C. For the composition of (βZr) at this reaction we take the value 22.5 at.% Al from the expression given above for the (βZr)/[(βZr) + Zr_2Al] boundary.

[61Wil] and [62Pot] determined the crystal structure of Zr_2Al to be of the hexagonal $InNi_2$-type.

Zr_5Al_3

Metallographic and thermal analysis of as-cast and annealed samples allowed [54Mcp] to conclude that a stable intermediate compound of composition Zr_5Al_3 forms through the peritectic reaction L + Zr_3Al_2 ↔ Zr_5Al_3 at 1395 ± 10 °C. Also, [54Mcp] suggested and [62Pot] (metallography, X-rays) later confirmed that Zr_5Al_3 becomes metastable at low temperatures because of a eutectoid reaction Zr_5Al_3 ↔ Zr_2Al + Zr_3Al_2 at 1000 °C.

For the composition of the L phase at the L + Zr_3Al_2 ↔ Zr_5Al_3 peritectic reaction, [54Mcp] suggested the approximate value 37 at.% Al. However, this value implies a large difference between the Zr_3Al_2 and Zr_5Al_3 liquidus slopes, a feature which is thermodynamically implausible. To attend this point, and compatible with the experimental observations made by [54Mcp] (see Fig. 3), we finally select 1400 °C for this peritectic temperature and tentatively adopt 35 at.% Al for the corresponding composition of the L phase.

A discrepancy existed regarding the crystal structure of Zr_5Al_3. [59Wil2] suggested a hexagonal Mn_5Si_3-type structure for this compound. However, [60Eds] and [62Pot] agreed that the crystal structure of Zr_5Al_3 is of the tetragonal Si_3W_5-type and, moreover, [60Eds] proved that the contamination with interstitial impurities stabilizes the Mn_5Si_3-type structure. More recently, [83Sch] (X-rays) confirmed the tetragonal structure for the Zr_5Al_3 phase at temperatures >800 °C but proposed the hexagonal structure for lower temperatures. Hence, according to Fig. 1, the hexagonal Mn_5Si_3-type structure would be a low- temperature, metastable form of pure Zr_5Al_3. [83Sch] also mentioned that this hexagonal form of Zr_5Al_3 seems to be strongly stabilized by interstitial impurities. Contrary to these conclusions, [88Kim] (X-rays) reported the hexagonal structure in the range 800 to 1100 °C and suggested that this is the true stable structure of Zr_5Al_3; however, their results might have been affected by the superficial contamination of their samples.

Zr_3Al_2

The existence of this intermediate compound was established by [54Mcp] by means of the metallographic analysis of as-cast samples. These authors used thermal analysis to determine that Zr_3Al_2 forms peritectically at 1480 ± 10 °C. [54Mcp] evaluated the composition of L at this peritectic reaction to be ~39 at.% Al. These values are those shown in Fig. 1. The crystal structure of the Zr_3Al_2 compound was reported to be tetragonal by [60Wil1] and [62Pot].

Zr_4Al_3 and Zr_5Al_4

[54Mcp] (metallography, thermal analysis) proposed the existence of an intermediate compound whose composition is close to Zr_4Al_3 and which melts congruently at 1530 ± 10 °C. This composition was later investigated by [62Pot] (X-rays, metallography) who concluded from crystal structure determinations that the correct composition for this compound is Zr_5Al_4 with a hexagonal crystal structure isotypic to that of Ga_4Ti_5. However, [60Wil2] confirmed the existence at low temperatures of a stable hexagonal structure with the composition Zr_4Al_3. This last intermediate phase was also observed by [62Pot] who investigated the structural changes of alloys close to the composition Zr_5Al_4 upon annealing around 1000 °C. The later authors then tentatively rationalized the available experimental information by suggesting the existence of (1) a peritectoid reaction Zr_3Al_2 + Zr_5Al_4 ↔ Zr_4Al_3 at ~1030 °C, and (2) a Zr_5Al_4 ↔ Zr_4Al_3 + ZrAl eutectoid reaction at ~1000 °C (see Fig. 1).

The assessed temperature of 1550 °C for the congruent melting of Zr_5Al_4 shown in Fig. 1 is consistent with the upper thermal arrests found by [54Mcp] for alloys of composition 42.7 and 49.1 at.% Al (see Fig. 3).

More recent work by [83Sch] (X-rays) and [84Kem, 85Kem] (X-rays) confirmed the features of the Zr-Al phase diagram which have been described above.

[54Mcp] (metallography, thermal analysis) indicated the existence of a eutectic reaction L ↔ Zr_5Al_4 + Zr_2Al_3 which occurs at 1485 ± 10 °C with a L composition of ~49 at.% Al (Zr_5Al_4 is designated as Zr_4Al_3 in [54Mcp]). However, [54Mcp] reported one and two thermal arrests for alloys containing 51 and 49 at.% Al, respectively (see Fig. 3). Therefore, in Fig. 1 we adopt the value 51 at.% Al for this eutectic composition; the same choice was made by [62Pot].

ZrAl

[54Mcp] (metallography, thermal analysis) examined alloys of composition close to 50 at.% concluding that a compound ZrAl forms at 1250 ± 50 °C through the peritectoid reaction Zr_5Al_4 + Zr_2Al_3 ↔ ZrAl. Later work by [62Pot] (metallography, X-rays), [83Sch] (X-rays), [84Kem] (X-rays), and [85Kem] (X-rays) confirmed the peritectoid formation of ZrAl. Because

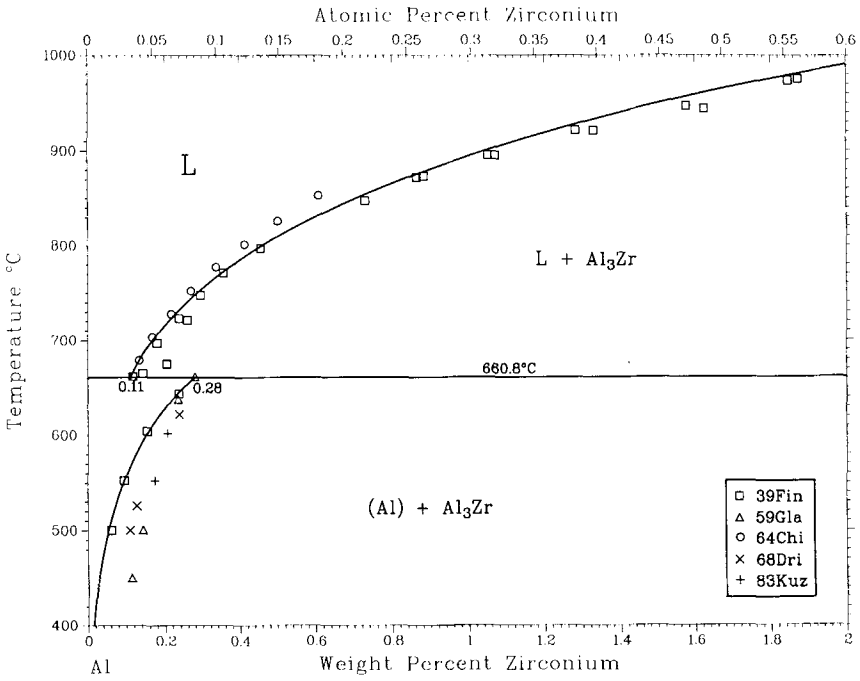

Fig. 4 Al-rich side of the Zr-Al phase diagram. Curves are calculated from Gibbs energy functions.

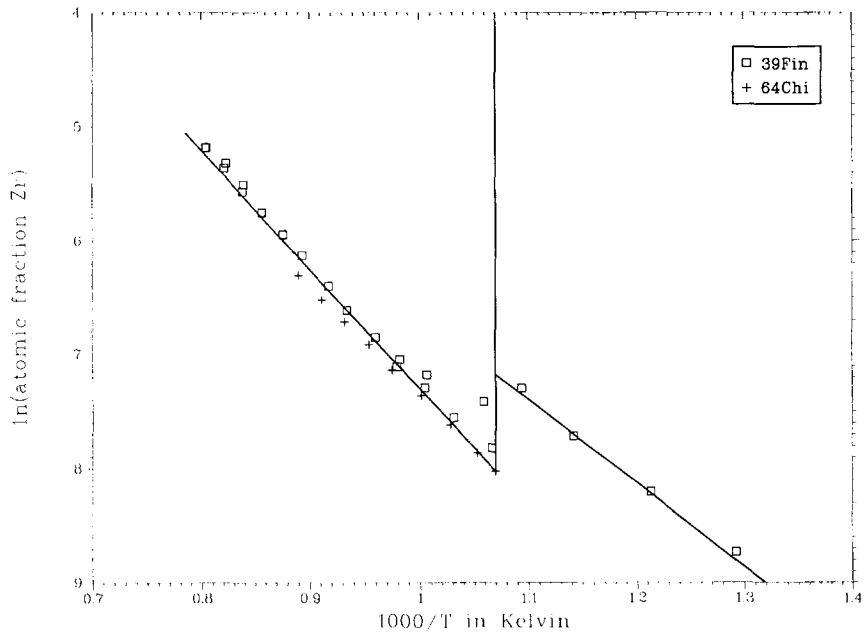

Fig. 5 Al-rich side of the Zr-Al phase diagram. Plotted as ln (atomic fraction Zr) vs 1000/T, where T is the temperature in K.

the results of [83Sch] suggested that ZrAl should remain stable up to 1300 °C, in Fig. 1 we adopt for the peritectoid temperature the value 1275 ± 25 °C as a compromise between the works of [54Mcp] and [83Sch]. The crystal structure of ZrAl was determined by [62Spo] to be of the orthorhombic BCr-type.

Zr_2Al_3

The existence of this compound was reported by [54Mcp] (metallography, thermal analysis). These authors also reported the existence of the peritectic reaction L + $ZrAl_2$ ↔ Zr_2Al_3 which occurs in the temperature range 1585 to 1605 °C with a L composition of ~59 at.% Al. The peritectic temperature shown in Fig. 1 is 1590 °C (see also Fig. 3). [61Ren] and [62Pot] established that the structure of Zr_2Al_3 is orthorhombic. [83Sch], [84Kem], and [85Kem] confirmed this result as well as the high temperature stability of Zr_2Al_3.

$ZrAl_2$

This intermediate compound was reported by [54Mcp] (metallography, thermal analysis) to melt congruently at 1645 ± 10 °C. However, this temperature strictly corresponds to the thermal arrest shown by a 68.8 at.% Al sample. Therefore, and as indicated in Fig. 3, we slightly modify the assessed melting temperature of $ZrAl_2$ and take in Fig. 1 the value 1660 °C.

[59Wil1] (metallography, X-rays) corroborated the congruent formation of $ZrAl_2$ and determined its crystal structure to be of the $MgZn_2$-type. [62Pot], [83Sch], and [84Kem] confirmed the structural results of [59Wil1].

$ZrAl_3$

This compound, which is the Al-richest intermediate phase of the Zr-Al system, was first reported by [38Bra] (X-rays) who also established that its crystal structure is tetragonal. Work by [39Fin], [62Pot], [72Oha], [83Sch], and [84Kem] confirmed the existence of this phase. [54Mcp] (thermal analysis) determined that $ZrAl_3$ melts congruently at 1580 ± 10 °C.

[54Mcp] determined the existence of a eutectic reaction L ↔ $ZrAl_2$ + $ZrAl_3$ which occurs in the temperature range 1480 to 1500 °C with a L composition of ~73.5 at.% Al. However, these values impose a steep slope on the L/(L + $ZrAl_3$) boundary at the eutectic temperature, which implies special characteristics for the thermodynamic properties of the L phase. In turn, this steep slope also constrains the slope of L/(L + $ZrAl_2$) to be steep at the eutectic temperature. In order to minimize this feature of the Zr-Al phase diagram, and be compatible with the presently available experimental information [54Mcp], we tentatively place in Fig. 1 the temperature of the L ↔ $ZrAl_2$ + $ZrAl_3$ eutectic reaction at 1500 °C and take for the L composition the more symmetrical value of 72 at.% Al. This last composition value is consistent with the single thermal arrest observed by [54Mcp] in a sample containing 71.3 at.% Al (see Fig. 3). Further experimental investigation of this feature of the Zr-Al phase diagram is necessary.

Al-Rich Alloys

Zr is an important minor alloying addition to Al-based alloys, and therefore the Al-rich side of the diagram up to 1000 °C is accurately known. Solubilities of Zr in both liquid and solid Al were definitively determined by [39Fin]. The liquid solubilities were determined from settling tests; the solid solubilities were determined from resistivity data and verified by metallography; the peritectic temperature was determined by thermal analysis on both heating and cooling. The assessed diagram on the Al-side (Fig. 4) is drawn from a thermodynamic calculation in which Gibbs energies on the Al-side were optimized with respect to the [39Fin] data. Solid (Al) forms from the liquid by the peritectic reaction L + $ZrAl_3$ ↔ (Al) at 660.8 °C. The maximum solubility of Zr in solid (Al) is 0.083 at.%; the composition of the liquid in the peritectic equilibrium is 0.033 at.% Zr. The present thermodynamic calculations verify the validity of the dilute limit approximation for the Al liquidus and solvus up to 1000 °C, as suggested by the linear relationship between the logarithm of the solubility and $1/T$ in K (see Fig. 5).

Solubilities of Zr in liquid Al were also measured by [64Chi] using the settling technique (equilibrated liquid was decanted and analyzed). The results were reported in the form of the equation

$$\log_{10}X = A/T + B$$

$$A = -4089 \pm 316$$

$$B = 0.896 \pm 0.305$$

where X is the atom fraction of Zr, T is the temperature in K, and the equation is valid between 660 and 850 °C.

Solid solubilities were also reported by [59Gla], [68Dri], and [83Kuz]; parametric methods based on microhardness data were used to determine the solvus compositions. The reported solubilities from these studies are somewhat higher than the selected values. The data are compared with the assessed boundaries in Fig. 4.

Metastable Phases

[73Car] observed the solubility of Al in (αZr) to be extended to at least 3 at.% Al alloy by quenching from the stable (αZr) field at 850 °C. According to [78Muk1] and [78Muk2], fast quenching from the (βZr) field of a 14 at.% Al alloy annealed at 1150 °C resulted in the formation of a cph supersaturated martensite which includes $D0_{19}$ microdomains. [76Sch] reported the extension of the (αZr) phase up to compositions 6 to 10 at.% Al after quenching from the L phase alloys containing 22 to 27 at.% Al.

[83Ban] (transmission electron microscopy, X-rays) investigated the sequence of transformations taking place in a 27 at.% Al alloy during rapid quenching from the liquid state. They found that the eutectic formation of Zr_5Al_3 is suppressed and that the structure of the as-quenched sample consists of a diffusion less-solidified (βZr) matrix, athermal-ω particles and Zr_2Al precipitates. The orientation and morphology of the Zr_2Al precipitates are closely related to the matrix, suggesting a formation mechanism which combines a spinodal separation of (βZr) and a hybrid displacive-replacive ordering reaction.

Disordering and eventual amorphization of Zr_3Al by ion irradiation were reported by [77How], [79How], and [87Reh]. [73Wil] studied the disordering effects of fast-neutron irradiation on Zr_4Al_3.

As discussed under the section "Zr_5Al_3," the hexagonal Mn_5Si_3-type structure would be a low temperature metastable form of the

Table 2 Zr-Al Crystal Structure Data

Phase	Composition, at.% Al	Pearson symbol	Space group	Strukturbericht designation	Prototype	Reference
(αZr)	0 to 10.5	*hP*2	$P6_3/mmc$	*A*3	Mg	[Massalski1]
(βZr)	0 to 26	*cI*2	$Im\bar{3}m$	*A*2	W	[Massalski1]
Zr_3Al	25	*cP*4	$Pm\bar{3}m$	$L1_2$	$AuCu_3$	[55Kee, 62Pot]
Zr_2Al	33.3	*hP*6	$P6_3/mmc$	$B8_2$	Ni_2In	[61Wil, 62Pot]
Zr_5Al_3	37.5	*tI*32	$I4/mcm$	$D8_m$	W_5Si_3	[60Eds, 62Pot, 83Sch, 85Kem]
Zr_3Al_2	40	*tP*20	$P4_2/mmm$	...	Al_2Zr_3	[60Wil1, 62Pot, 85Kem]
Zr_4Al_3	42.9	*hP*7	$P\bar{6}$	...	Al_3Zr_4	[60Wil2, 62Pot, 85Kem]
Zr_5Al_4	44.4	*hP*18	$P6_3/mcm$	...	Ga_4Ti_5	[62Pot]
ZrAl	50	*oC*8	*Cmcm*	B_f	CrB	[62Spo, 85Kem]
Zr_2Al_3	60	*oF*40	*Fdd*2	...	Al_3Zr_2	[62Pot, 85Kem]
$ZrAl_2$	66.7	*hP*12	$P6_3/mmc$	*C*14	$MgZn_2$	[59Wil, 62Pot]
$ZrAl_3$	75	*tI*16	*I*4/*mmm*	$D0_{23}$	Al_3Zr	[38Bra, 85Kem]
(Al)	99.93 to 100	*cF*4	$Fm\bar{3}m$	*A*1	Cu	[Massalski1]

pure compound Zr_5Al_3. Lattice parameters for this hexagonal structure are: $a = 0.8170$ nm, $c = 0.5655$ nm [83Sch]. For the dependence of the lattice parameters of hexagonal Zr_5Al_3 with oxygen contamination, see [88Cla].

Amorphous Zr-Al films were produced within the eutectic compositions 26 to 37 and 47 to 55 at.% Al by [75Gud]. This author also reported the retention of metastable (bZr) up to ~26 at.% Al.

Supersaturated solid solutions of Zr in (Al) containing as much as 3 at.% Zr can be prepared by rapid solidification [84Cha1, 87Pan], and considerable supersaturation is also achieved in more dilute cast alloys. A coherent phase $mZrAl_3$ with the ordered fcc $L1_2$ structure [69Izu, 69Ryu, 72Nes, 87Vec] precipitates as a metastable phase from the supersaturated solution. [87Vec] measured the composition of $mZrAl_3$ by energy dispersive X-ray spectrometry; they found it to form off-stoichiometry, at 16.5 at.% Zr.

From studies with thin films, [84Cha2] reported the precipitation of metastable cubic-Zr_2Al_{11} and orthorhombic-$ZrAl_6$ compounds after annealing of supersaturated (Al) solid solutions containing ~3 at.% Zr. From similar studies, [87Pan] confirmed the results of [84Cha2] and, in addition, reported the formation of metastable cubic-ZrAl and a vacancy-ordered phase based on ZrAl. The metastable cubic-$mZrAl_3$ normally obtained following melt quenching was not observed by [84Cha2] or [87Pan].

$mZrAl_3$ is responsible for the effectiveness of Zr to control recrystallization in Al-based alloys. It causes more uniform distribution of dislocations and it pins grain and subgrain boundaries [69Ryu]; $mZrAl_3$ is very stable against coarsening and against redissolution [77Dah2].

$mZrAl_3$ also forms from the melt as a primary phase during rapid solidification [72Oha, 77Dah1]. $mZrAl_3$ crystals act as nuclei for solidification of (Al), and Zr can thus work as a grain refiner of Al [77Dah1, 81Hor]. According to [86Pan], solidification of $mZrAl_3$ is preceded by another metastable phase during rapid solidification of a 98.1 at.% Al alloy.

The coherent solvus for precipitation of $mZrAl_3$ would be valuable for predicting volume fractions of dispersoid; however based on the literature data, it can only be crudely estimated. Two experiments to determine the coherent $mZrAl_3$ solvus have been reported. [72Cer] measured low temperature resistivities of pure Al, of a 0.5 at.% Zr alloy quenched from the homogenization temperature, and of a 0.5 at.% Zr alloy quenched from a long precipitation anneal at 350 °C. Assuming that the resistivities are simply proportional to the amount of Zr in solution, a matrix composition of 0.049 at.% Zr was calculated. [86Zed] measured the lattice parameter of the matrix phase at 425 °C for two-phase (Al) + $ZrAl_3$ and (Al) + $mZrAl_3$ alloys. Taking 0.0055 at.% Zr for the equilibrium solvus composition at 425 °C, metastable solvus composition of 0.008 at.% Zr at 425 °C is calculated.

These two results are clearly inconsistent. The lower solubility [86Zed] is preferred because fewer questionable assumptions are required to interpret a measurement made at temperature. The coherent $mZrAl_3$ solvus was modeled thermodynamically by [88Sau] and as part of this work. Although very different approaches were taken to the problem, the results agree reasonably well with each other and with the [86Zed] measurement (see Fig. 6). Details of the calculations and suggested critical experiments are discussed in the section "Thermodynamics" of this evaluation.

Crystal Structures and Lattice Parameters

Zr-Al crystal structure data are summarized in Table 2. Lattice parameter data for (αZr) and all the intermediate phases are shown in Table 3. [62Eds] pointed out similarities between the structures of Zr-Al intermetallics and those of the silicides and borides. For example, Zr_4Al_3 has a σ-phase-like structure, related to the sigma phases Ta_2Al and Nb_2Al. The Zr_2Al structure belongs to the NiAs family of silicide-like phases.

[80Stu] estimated the effect of Zr on the lattice parameter of Al as

$$a(x) = a(\text{Al}) + 0.000507x$$

where a is the lattice parameter in nm and x the composition of Zr in at.%.

Table 3 Zr-Al Lattice Parameter Data at Room Temperature

Phase	Composition, at.% Al	Lattice parameters, nm a	b	c	Comment	Reference
(αZr)	0	0.32316	...	0.51475	...	[Massalski1]
	0.555	0.32309	...	0.51419	(a)	[70Tiw]
	2.800	0.32212	...	0.51365	(a)	[70Tiw]
	4.167	0.32140	...	0.51310	(a)	[70Tiw]
	5.242	0.32103	...	0.51247	(a)	[70Tiw]
βZr	0	0.36090	...	...	>863 °C	[Massalski1]
Zr_3Al	25	0.4373	...	...	...	[55Kee, 62Pot]
Zr_2Al	33.3	0.4882	...	0.5918	...	[62Pot]
Zr_5Al_3	37.5	1.1042	...	0.5393	(b)	[62Pot, 85Kem, 88Cla]
Zr_3Al_2	40	0.7632	...	0.6997	(b)	[60Wil1, 85Kem]
Zr_4Al_3	42.9	0.5430	...	0.539	...	[60Wil2, 85Kem, 60Eds]
Zr_5Al_4	44.4	0.844	...	0.5785	(c)	[62Pot, 85Kem]
ZrAl	50	0.3360	1.0890	0.427	...	[62Spo, 62Pot, 85Kem]
Zr_2Al_3	60	0.9601	1.391	0.5578	...	[61Ren, 62Pot, 85Kem]
$ZrAl_2$	66.7	0.5280	...	0.8747	...	[59Wil, 85Kem]
$ZrAl_3$	75	0.4010	...	1.730	...	[38Bra, 62Pot, 85Kem]
Al	100	0.40496	...	...	...	[Massalski1]

Note: The listed values are averages from cited references. Samples previously heat treated at: **(a)** 850 °C, **(b)** 1100 °C, **(c)** 1100 to 1200 °C.

Table 4 Enthalpy of Formation of Zr-Al Intermediate Compounds

Reference	Enthalpy of formation, kJ/mol of atoms Zr_3Al	Zr_2Al	Zr_5Al_3	Zr_3Al_2	Zr_5Al_4	ZrAl	Zr_2Al_3	$ZrAl_2$	$ZrAl_3$	Comment
[84Kem]	...	...	−39	−41	−44	−45	−47	−46	−41	(a)
[84Kem](b)	...	...	−48	−49	−52	−53	−55	−54	−49	(a)
[76Alc]	...	...	...	...	...	...	−31 ± ?	−44 ± 2	−44 ± 2	(c)
[88Boe]	−50	−65	−72	−75	...	−83	−80	−72	−57	...

(a) Standard states at 298 K. Estimated errors are ± 4 kJ/mol of atoms. **(b)** [84Kem] values corrected by present authors. See text. **(c)** Standard states at 1000 K.

Thermodynamics

Experimental Data

[84Kem] determined the enthalpies of formation of Zr_5Al_3, Zr_3Al_2, Zr_5Al_4, ZrAl, Zr_2Al_3, $ZrAl_2$, and $ZrAl_3$. These authors measured the Al vapor pressure of alloys from pure Zr up to 75 at.% Al in the temperature range 1025 to 1400 °C by means of a Knudsen cell mass spectrometric technique. With assumption of the validity of the Neumann-Kopp rule, use of the Gibbs-Duhem equation, and neglect of any effects of possible nonstoichiometry of the intermetallic compounds, the standard enthalpy changes of the following decomposition reactions were determined by [84Kem] by means of the second- and third-law methods:

$$\frac{1}{3}Zr_5Al_3 \rightarrow \frac{5}{3}Zr(g) + Al(g)$$

$$\frac{1}{3}Zr_5Al_3 \rightarrow \frac{5}{3}Zr(\beta Zr) + Al(g)$$

$$5Zr_3Al_2 \rightarrow 3Zr_5Al_3 + Al(g)$$

$$\frac{3}{2}Zr_5Al_4 \rightarrow \frac{5}{2}Zr_3Al_2 + Al(g)$$

$$\frac{5}{7}Zr_2Al_3 \rightarrow \frac{2}{7}Zr_5Al_4 + Al(g)$$

$$Zr_2Al_3 \rightarrow 2ZrAl + Al(g)$$

$$2ZrAl_2 \rightarrow Zr_2Al_3 + Al(g)$$

$$ZrAl_3 \rightarrow ZrAl_2 + Al(g)$$

These enthalpy changes were in turn used by [84Kem] to calculate the standard enthalpies of formation, $\Delta_f H^0_{298}$, of the corresponding intermetallic compounds; the results obtained are listed in Table 4. [84Kem] did not take into account the difference between the free energies of the liquid and solid phases of pure Al above its melting point; therefore, we have re-calculated the $\Delta_f H^0_{298}$ values adopting for $\Delta C_p = C_p$

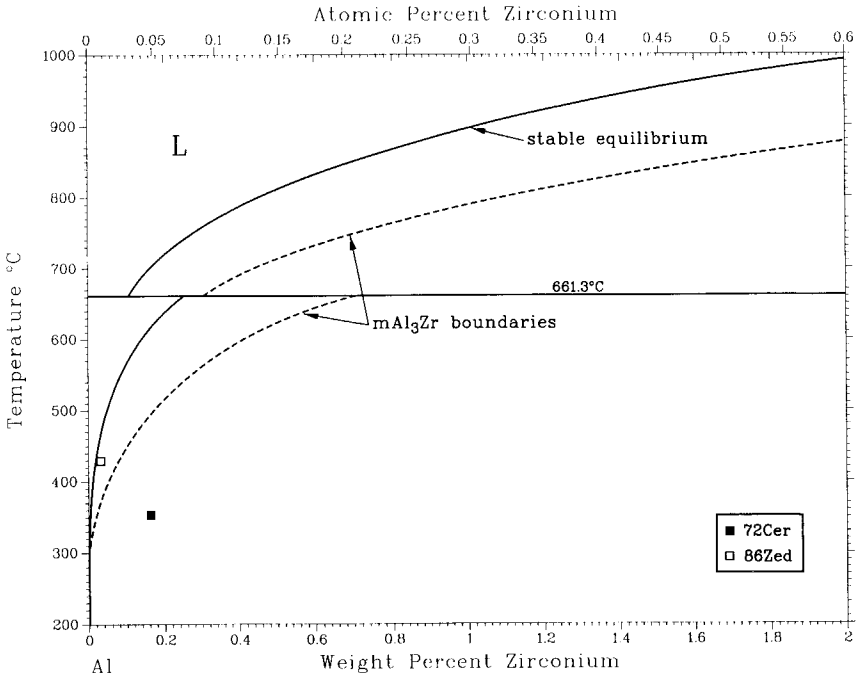

Fig. 6 Rough estimate for the coherent metastable $L1_2$ phase $mZrAl_3$.

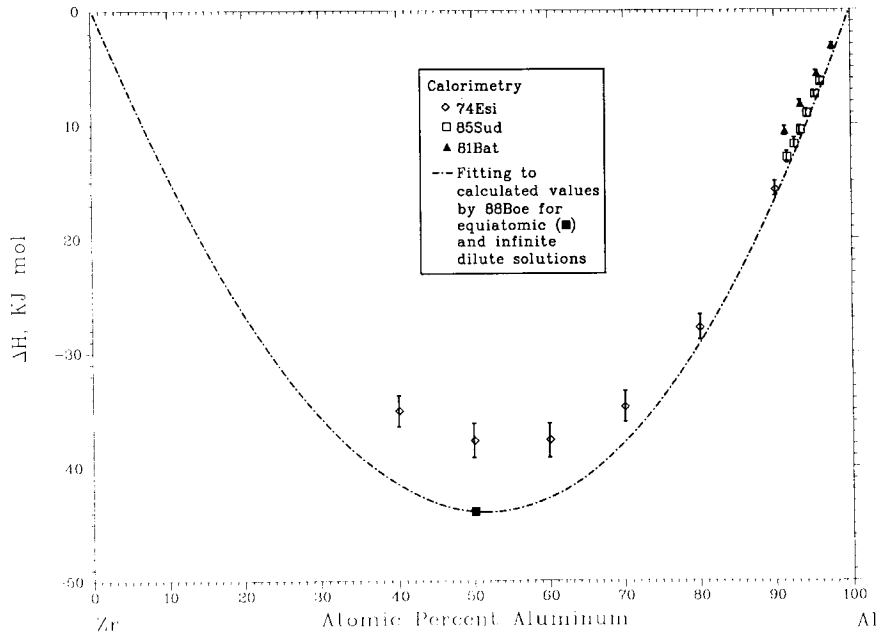

Fig. 7 Enthalpy of formation of Zr-Al liquid solutions.

(liquid Al) – C_p(fcc Al), $T > T_m$, the values provided by the SGTE data base. The corrected values obtained for $\Delta_f H^0_{298}$ are listed in Table 4. For comparison, some calorimetric values for $\Delta_f H$ quoted in [76Alc], obtained through a private communication, are also listed in Table 4.It should be mentioned that the temperature range in which [84Kem] studied the reaction

$$\frac{1}{3}Zr_5Al_3 \leftrightarrow \frac{5}{3}Zr(\beta Zr) + Al(g)$$

namely 1220 to 1305 °C, may imply the precipitation of the compound Zr_2Al. This would introduce systematic errors in the thermodynamic values computed by [84Kem]. Also, the later authors found a discrepancy for the values of the enthalpy of the reaction

$$\frac{3}{2}Zr_5Al_4 \leftrightarrow \frac{5}{2}Zr_3Al_2 + Al(g)$$

when evaluated by means of the second- or third-law methods. This discrepancy may be due to a failure of the Neumann-Kopp rule assumed by [84Kem].

[61Sch] (solubility measurements) determined values of $\Delta_f G$ for three intermetallic compounds, as follows:

$\Delta_f G$ (Zr_4Al_3, s, 740 °C) = –43.1 kJ/mol of atoms

$\Delta_f G$ (Zr_2Al_3, s, 740 °C) = –53.5 kJ/mol of atoms

$\Delta_f G$ ($ZrAl_2$, s, 740 °C) = –56.9 kJ/mol of atoms

The experimental procedure technique used by [61Sch] was criticized by [Hultgren,B].

[74Esi], [81Bat], and [85Sud] measured the enthalpies of mixing of liquid alloys using calorimetric techniques. Good agreement exists among the results of these authors, which are shown in Fig. 7.

With an electrochemical technique, [82Bat] measured the activity of Al at 850 °C in Al-rich liquid alloys. The solubility limit of Zr in liquid Al proposed by [82Bat] at this temperature is ~1.3 at.% Zr which is much larger than the assessed value of 0.2 at.% Zr (see Fig. 4). Therefore, the validity of the results obtained by [82Bat] are questioned and not further considered in this evaluation.

[86Sau] initially modeled and later revised [88Sau] Gibbs energies for the Zr-Al system. The revisions bring about consistency with SGTE thermodynamic properties of the elements and somewhat improve the agreement with the phase diagram on the Al-side. However, [86Sau] already noted that their modeling could not represent the experimental value of 1490 °C for the temperature of the L ↔ $ZrAl_2$ + $ZrAl_3$ eutectic reaction. Hence, [86Sau] suggested that the experimental eutectic temperature is 80 °C too low. If the stated experimental eutectic temperature is, as we think, essentially correct, the Redlich-Kister-type expansion used by [86Sau] would not be adequate to describe this part of the Zr-Al phase diagram (for example, a tendency to association may exist in the liquid phase).

For modeling low-level Zr additions to multicomponent Al alloys, very precise results are needed for the Al-rich liquidus and solidus, and therefore a set of Gibbs energies modified from the version of [86Sau] were constructed as part of this work. In the present calculations, the Gibbs energy of a solution phase φ is represented as

$$G\varphi(X,T) = G^0(\mathrm{Al})(1-X) + G^0(\mathrm{Zr})X + RT[X\ln X + (1-X)\ln(1-X)] + \sum_i X(1-X)\,P_i(1-2X)\,A_i(T)$$

where X is the atom fraction Zr, G^0 is the lattice stability of the pure elements, P_i is the i^{th} Legendre polynomial, and A_i is an empirically-determined coefficient that may be a function of temperature. The A_i is optimized with respect to the combined thermodynamic and phase diagram data. All the intermetallic phases, including the metastable $L1_2$ m$ZrAl_3$ phase, are modeled as strictly stoichiometric. Parameters of the resulting Gibbs energy functions are listed in Table 5.

Figure 8 compares partial and integral enthalpies of mixing of the liquid from [74Esi], [82Bat], and [85Sud] with the results of the present calculations. The value of the partial molar enthalpy, H_{Zr}, in the dilute limit is derived from the phase diagram together with the $ZrAl_3$ enthalpy of formation. This value is consistent with the scattered measurements.

The calculated phase diagram is compared with experiment in Fig. 4, 6, and 9. Three features of the calculated phase diagram are

Table 5 Gibbs Energies of the Zr-Al System, J/mol, J/K·mol

Lattice stability parameters

G^0(Al, L) = 10 711 – 11.4728 T
G^0(Zr, L) = 22 092 – 12.1340 T
G^0(Al, bcc) = 10 083 – 4.8120 T
G^0(Zr, bcc) = 4 310 – 3.7660 T
G^0(Al, cph) = 4 286 – 1.4070 T
G^0(Zr, cph) = 0
G^0(Al, fcc) = 0
G^0(Zr, fcc) = 3 348

Solution phase interaction parameters

Phase	Term	Coefficient
L	ZrAl*	–157 186 + 66.896 T
L	Zr*Al*P_1(Zr-Al)	20 447
bcc	ZrAl*	–111 944 + 32.196 T
	Zr*Al*P_1(Zr-Al)	–7332
cph	ZrAl*	–112 300 + 32.196 T
	Zr*Al*P_1(Zr-Al)	–7332
fcc	ZrAl*	–111 692 + 40.710 T

Standard Gibbs energies of intermetallic phases

G($ZrAl_3$) = –44 298 + 11.590 T
G(m$ZrAl_3$) = –40 300 + 11.590 T
G($ZrAl_2$) = –45 536 + 12.037 T
G(Zr_2Al_3) = –45 200 + 11.448 T
G(ZrAl) = –44 685 + 11.328 T
G(Zr_5Al_4) = –43 127 + 10.426 T
G(Zr_3Al_2) = –40 564 + 9.763 T
G(Zr_5Al_3) = –39 000 + 9.372 T
G(Zr_2Al) = –39145 + 11.026 T
G(Zr_3Al) = –31767 + 9.666 T

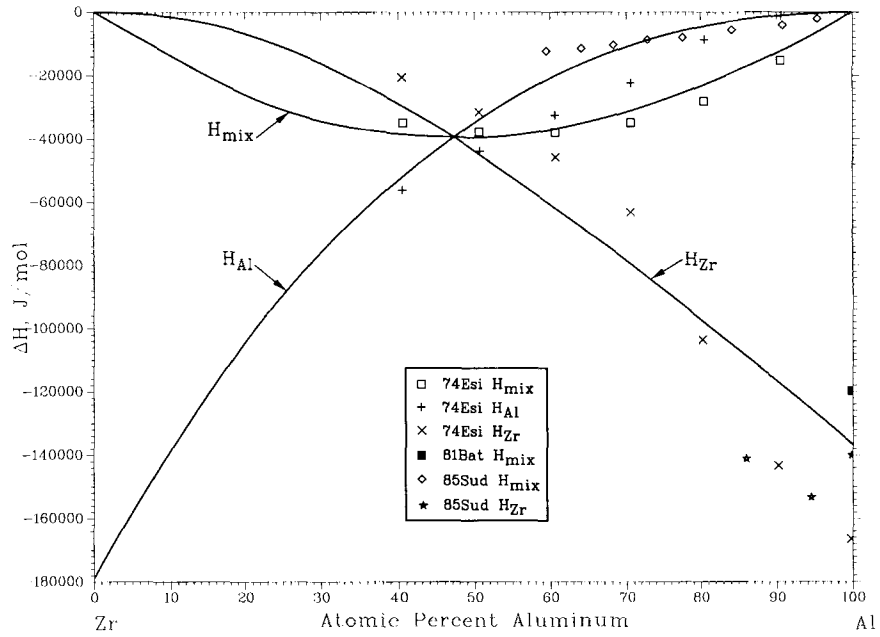

Fig. 8 Partial and integral enthalpies of mixing for the liquid phase, according to experiments and to the present calculations.

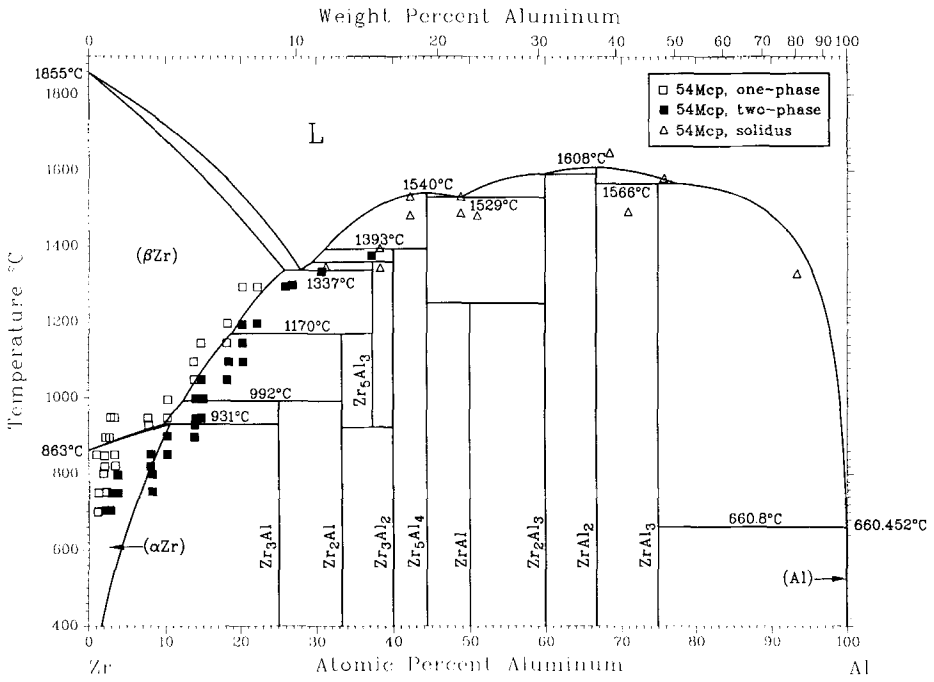

Fig. 9 Zr-Al phase diagram calculated from the Gibbs energy functions listed in Table 5.

noteworthy. (1) Compared to the liquidus curves constructed by [54Mcp] from the experimental data, the liquidus of each intermetallic compound near its congruent melting point is rather flat and symmetrical about stoichiometry. This feature appears in all calculations of the Zr-Al system (*e.g.* [86Sau] and [88Sau]). A better fit to the curves proposed by [54Mcp] would require a more complicated model for the L. Further experimental work is needed regarding the liquidus of the Zr-Al system. (2) The temperature dependence of the (αZr) solvus is not reproduced by the calculation. This feature also shows up in the calculation by [88Sau]. It is probably a failure of the models; in the absence of liquidus, solidus, or enthalpy data for (βZr), severe constraints must be imposed on coefficients of the solution phase to prevent singularities in the phase boundaries. (3) On the Al-rich side, the agreement between calculated diagram and experimental data is excellent. In particular the calculation demonstrates the consistency among the peritectic temperature, the compositions of liquid and solid Al, and the enthalpy of melting of Al, as required by the Gibbs-Konovalov relationship.

Because there are only two (inconsistent) data for the coherent $mZrAl_3$ solvus, that boundary can only be calculated from a predictive model. [88Sau] used the Gibbs energy for the disordered fcc (Al) solution, as derived from the stable equilibrium diagram, to construct the Gibbs energy of the ordered $L1_2$ phase in the Bragg-Williams approximation. He found that $mZrAl_3$ has a congruent melting point only 50 °C below that of the stable equilibrium phase, *i.e.*, it is very nearly a stable phase. Calculated metastable solvus compositions were reported to be 0.3 at.% Zr at 660 °C and < 0.004 at.% Zr at 200 °C.

In the present work, it was desired to model $mZrAl_3$ as a line compound in order to extend the calculations easily to a variety of multicomponent systems. It was assumed that only an enthalpy term, and no entropy term, contributes to the Gibbs energy difference between the stable and metastable phases. This guarantees that $mZrAl_3$ does not become an equilibrium phase at high temperature. The enthalpy difference between the two compounds was assumed to arise from the coherency of $mZrAl_3$ with the matrix. From the elastic properties of Al and the estimate by [80Stu] for the composition dependence of the lattice parameter, an elastic energy of 2000 J/mol was calculated.

The calculated metastable phase boundaries are shown in Fig. 6. The calculated solvus is somewhat higher in Zr than the value taken from the [86Zed] work, but much lower than the value reported by [72Cer]. The calculated solid solubility is lower than predicted by [88Sau], but at high temperature the liquid solubility becomes higher. Finally the calculated metastable peritectic reaction occurs at 661.3 °C, with liquid and solid compositions of 0.09 and 0.21 at.% Zr respectively. The calculated peritectic liquid composition lies within the range where the grain refining effect of Zr begins.

Measurement of the metastable peritectic temperature during slow cooling of very fine droplets suggests itself as a critical experiment for refinement of the metastable phase boundaries. Direct measurement of the metastable solvus should involve a direct quench from the homogenization temperature in order to avoid erroneously high solvus temperatures due to slow kinetics of dissolution of $mZrAl_3$ previously formed at lower temperature.

[88Boe] presented a phenomenological calculation of $\Delta_f H$(Zr-Al) for various compositions. The results obtained for the solid and liquid phases are shown in Table 4 and Fig. 7, respectively.

Cited References

38Bra: G. Brauer, "Crystal Structure of Intermetallic Alloys of Aluminium with Titanium, Zirconium, Thorium, Niobium and Tantalum," *Naturwissenschaften, 26*, 710 (1938) in German. (Crys Structure; Experimental)

***39Fin:** W.L. Fink and L.A. Willey, "Equilibrium Relations in Aluminium-Zirconium Alloys of High Purity," *Met. Technol., 1*, 69-80 (1939). (Equi Diagram, Thermo; Experimental)

***54Mcp:** D.J. McPherson and M. Hansen, "The System Zr-Al," *Trans. ASM, 46*, 354-374 (1954). (Equi Diagram; Experimental; #)

55Kee: H.H. Keeler and J.H. Mallery, "Crystal Structure and Some Properties of the Compound, Zr_3Al," *J. Met., 2*, 394 (1955) (Crys Structure; Experimental)

59Gla: V.M. Glazov, G. Lazarev, and Korolkov, "The Solubility of Certain Transition Metals in Aluminium," *Metalloved. Term. Obrab. Met., 10*, 48-50 (1959). (Equi Diagram; Experimental)

59Wil1: C.G. Wilson, "The Crystal Structure of $ZrAl_2$," *Acta Crystallogr., 12*, 660-662 (1959). (Equi Diagram, Crys Structure; Experimental)

59Wil2: C.G. Wilson, D. Sams, and T.J. Renouf, "The Crystal Structure of Zr_5Al_3," *Acta Crystallogr., 12*, 947-948 (1959). (Equi Diagram, Crys Structure; Experimental)

***60Eds:** L.E. Edshammar and S. Andersson, "Studies on the Zirconium-Aluminium and Hafnium-Aluminium Systems," *Acta Chem. Scand., 14*(1), 223-224 (1960). (Equi Diagram, Crys Structure; Experimental)

60Wil1: C.G. Wilson and F.J. Spooner, "The Crystal Structure of Zr_3Al_2," *Acta Crystallogr., 13*, 358-359 (1960). (Equi Diagram, Crys Structure; Experimental)

60Wil2: C.G. Wilson, D.K. Thomas, and F.J. Spooner, "The Crystal Structure of Zr_4Al_3," *Acta Crystallogr., 13*, 56-57 (1960). (Equi Diagram, Crys Structure; Experimental)

61Ren: T.J. Renouf, "The Crystal Structure of Zr_2Al_3," *Acta Crystallogr., 14*, 469-472 (1961). (Equi Diagram, Crys Structure; Experimental)

61Sch: A. Schneider, H. Klotz, J. Stendel, and G. Strauss, "On the Thermochemistry of Alloys," *Pure Appl. Chem., 2*, 13-16 (1961). (Thermo; Experimental)

61Wil: C.G. Wilson and D. Sams, "The Crystal Structure of Zr_2Al," *Acta Crystallogr., 14*, 71-72 (1961). (Equi Diagram, Crys Structure; Experimental)

***62Eds:** L. Edshammar, "Crystal Structure Investigations on the Zr-Al and Hf-Al Systems," *Acta Chem. Scand., 16*, 20-30 (1962). (Equi Diagram; Experimental)

***62Pot:** M. Potzschke and K. Schubert, "On the Construction of Some T^4-B^3 Homologous and Quasihomologous Systems. II. The Ti-Al, Zr-Al, Hf-Al, Mo-Al and Some Ternary Systems," *Z. Metallkd., 53*(8), 548-561 (1962) in German. (Equi Diagram, Crys Structure, Thermo; Experimental; #)

62Spo: F.J. Spooner and C.G. Wilson, "The Crystal Structure of ZrAl," *Acta Crystallogr., 15*, 621-622 (1962). (Equi Diagram, Crys Structure; Experimental)

64Chi: P. Chiotti and P.F. Woerner, "Metal Hydride Reactions. I. Reaction of Hydrogen with Solutes in Liquid Metal Solvents," *J. Less-Common Met., 7*, 111-119 (1964). (Equi Diagram; Experimental)

68Dri: M.E. Drits, E.S. Kadaner, and V.I. Kuz'mina, "Solubility of Silicon and Zirconium in Aluminium," *Izv. Akad. Nauk, 1*, 102-105 (1968). (Equi Diagram; Experimental)

69Izu: O. Izumi and D. Oelschlagel, "On the Decomposition of a Highly Supersaturated Al-Zr Solid Solution," *Scr. Metall., 3*, 619-622 (1969). (Meta Phases; Experimental)

69Ryu: N. Ryum, "Precipitation and Recrystallization in an Al-0.5 wt.% Zr-Alloy," *Acta Metall., 17*, 269-278 (1969). (Meta Phases; Experimental)

70Tiw: S.N. Tiwari and K. Tangri, "The Solid Solubility of Aluminium in α-Zirconium," *J. Nucl. Mater., 34*, 92-96 (1970). (Equi Diagram; Experimental)

72Cer: S. Ceresara, M. Conserva, and P. Fiorini, "Recovery and Recrystallization of an Al-0.18 wt.% Zr Alloy Cold Worked at –196 °C," *Mater. Sci. Eng., 9*, 19-23 (1972). (Meta Phases; Experimental)

72Nes: E. Nes, "Precipitation of the Metastable Cubic Al_3Zr Phase in Subperitectic Al-Zr Alloys," *Acta Metall., 20*, 499-506 (1972). (Meta Phases; Experimental)

72Oha: T. Ohashi and R. Ichikawa, "A New Metastable Phase in Rapidly Solidified Al-Zr Alloys," *Metall. Trans., 3*, 2300-2302 (1972). (Equi Diagram, Meta Phases; Experimental)

73Car: G.J.C. Carpenter and J.F. Watters, "Vacancy Precipitation in Zirconium Alloys," *Acta Metall., 21*, 1207-1214 (1973). (Meta Phases; Experimental)

73Wil: C.G. Wilson, N. Wilson, V. Joksimovic, and J.A. Westphalen, "The Effect of Fast-Neutron Irradiation on Zr_4Al_3," *Acta Crystallogr., A, 29*, 336-341 (1973). (Meta Phases; Experimental)

74Esi: Yu.O. Esin, H. Bobrov, M. Petrushevskii, and B. Gel'd, "Enthalpies of Formation of Liquid Alloys of Al with Ti and Zr," *Izv. Akad. Nauk SSSR, Met., 5*, 104-109 (1974) in Russian. (Thermo; Experimental)

75Gud: V.N. Gudzenko and A.F. Polesya, "Structure of Zirconium-Aluminium Alloys Rapidly Cooled from the Liquid State," *Phys. Met. Metallogr., 39*, 177-179 (1975). (Meta Phases; Experimental)

75Sch: E.M. Schulson, D.H. McColl, and V.C. Ling, "Refinement of the Zr/Zr_2Al Duplex Structure in Zr-7.6 to -9.0 wt.% Al Ingots," Chalk River Nuclear Laboratories, AECL-5176, July 1975, Chalk River, Ontario, Canada. (Equi Diagram; Experimental; #)

76Alc: C.B. Alcock, K.T. Jacob, S. Zador, "Thermochemical Properties," *Zirconium: Physico-Chemical Properties of Its Compounds and Alloys,* O. Kubaschewski, Ed., Atomic Energy Review Special Issue No. 6, International Atomic Energy Agency, Vienna (1976). (Thermo; Review)

76Kub: O. Kubaschewski-von Goldbeck, "Phase Diagrams," *Zirconium: Physico-Chemical Properties of Its Compounds and Alloys,* O. Kubaschewski, Ed., Atomic Energy Review Special Issue No. 6, International Atomic Energy Agency, Vienna (1976). (Thermo; Review)

76Sch: E.M. Schulson and D.B. Graham, "The Peritectoid Formation of Ordered Zr_3Al," *Acta Metall., 24*, 615-625 (1976). (Equi Diagram; Experimental)

77Dah1: W. Dahl, W. Gruhl, W.G. Burchard, G. Ibe, and C. Dumitrescu, "Solidification and Precipitation Behavior of Al-Zr Alloys. I. The Influence of Zr on the Solidification Stucture," *Z. Metallkd., 68*, 121-127 (1977) in German. (Meta Phases; Experimental)

77Dah2: W. Dahl, W. Gruhl, W.G. Burchard, G. Ibe, and C. Dumitrescu, "Solidification and Precipitation Behavior of Al-Zr Alloys. II. Precipitation Processes in Al-Zr Alloys," *Z. Metallkd., 68*, 188-194 (1977) in German. (Meta Phases; Experimental)

77How: L.M. Howe and M.H. Rainville, "A Study of the Irradiation Behaviour of Zr_3Al," *J. Nucl. Mater., 68*, 215-234 (1977). (Meta Phases; Experimental)

78Muk1: P. Mukhopadhyay and V. Raman, "Discontinuous Precipitation in a Martensite," *Metallography, 11*, 481-485 (1978). (Meta Phases; Experimental)

78Muk2: P. Mukhopadhyay, V. Raman, S. Banerjee, and R. Krishnan, "Formation of a $D0_{19}$ Phase in Zirconium-Aluminium Martensites," *J. Mater. Sci., 13*, 2066-2068 (1978). (Meta Phases; Experimental)

79How: L.M. Howe and M.H. Rainville, "The Nature of Irradiation-Produced Damaged Regions in Ordered Zr_3Al," *Philos. Mag. A, 39*(2), 195-212 (1979). (Meta Phases; Experimental)

80Sch: E.M. Schulson, "Further Observations of the Peritectoid Transformation Zr + Zr_2Al Zr_3Al," *Metall. Trans. A, 11*, 1918-1920 (1980). (Equi Diagram; Experimental)

80Stu: H.C. Stumpf, Alcoa Laboratories, unpublished work (1980). (Crys Structure; Experimental)

81Bat: G.I. Batalin et al. "Heats of Solution of Ti, Zr and B in liquid Al," *Russ. Metall., 1*, 61-63 (1981). (Thermo; Theory)

81Hor: S. Hori, S. Saji, and A. Takehara, "Metastable Phase and Grain Refinement in Rapidly Al-Zr Alloys," *J. Jpn. Inst. Light Met., 31*(12), 793-797 (1981). (Meta Phases; Experimental)

82Bat: G.I. Batalin, E.A. Beloborodova, V.V. Nerubaschenko, V.D. Galodchka, and L.I. Slyuzko, "Thermodynamic Properties of Liquid Solution in the Aluminium-Zirconium System," *Izv. V. U. Z. Tsvetn. Metall., 3*, 74-77 (1982) in Russian. (Thermo; Experimental)

83Ban: S. Banerjee and R.W. Cahn, "An Ordered ω-phase in the Rapidly Solidified Zr-27at.% Al Alloy," *Acta Metall., 31*(10), 1721-1735 (1983). (Meta Phases; Experimental)

83Kuz: G.M. Kuznetsov, A.D. Barsukov, and M.I. Abas, "Solubility of Mn, Cr, Ti and Zr in Al in the Solid State," *Sov. Non-Ferrous Met. Res., 11* (1), 47-51 (1983). (Equi Diagram; Experimental)

***83Sch:** J.C. Schuster, J. Bauer, and J. Debuigne, "Investigation of Phase Equilibria Related to Fusion Materials: I. The Ternary System Zr-Al-N," *J. Nucl. Mater., 116*, 131-135 (1983). (Equi Diagram, Meta Phases, Crys Structure; Experimental)

84Cha1: Z.A. Chaudhury and C. Suryanarayana, "A TEM Study of Decomposition Behaviour of a Melt-Quenched Al-Zr Alloy," *Metallography, 17*, 231-252 (1984). (Meta Phases; Experimental)

84Cha2: Z.A. Chaudhury and C. Suryanarayana, "Transmission Electron Microscopy Studies of a Vapour-Deposited Al-Zr Alloy," *Mater. Sci. Eng., 67*, 47-53 (1984). (Meta Phases; Experimental)

***84Kem:** R.J. Kematick and H.F. Franzen, "Thermodynamic Study of the Zirconium-Aluminium System," *J. Solid State Chem., 54*, 226-234 (1984). (Equi Diagram, Thermo, Experimental; #)

85Kem: R.J. Kematick, "High Temperature Thermodynamics of the Zirconium-Aluminium System," Ph.D. Thesis, Iowa State University IS-T-1148, DE85 009230, 1985. (Equi Diagram, Crys Structure; Experimental; #)

85Sud: V.S. Sudavtsova, G.I. Batalin, and V.S. Tutevich, "Thermodynamic Properties of Molten Binary Alloys in Systems Al-Zr (Nb, Mo)," *Izv. Akad. Nauk SSSR, Met., 5*, 185-187 (1985), in Russian. (Thermo; Experimental)

86Pan: S.K. Pandey, D.K. Gangopadhyay, and C. Suryanarayana, "A Microstructural Study of Rapidly Quenched Al-Zr Alloys," *Z. Metallkd., 77*(1), 12-16 (1986). (Meta Phases; Experimental)

86Sau: N. Saunders and V.G. Rivlin, "Thermodynamic Characterization of Al-Cr, Al-Zr, and Al-Cr-Zr Alloy Systems," *Mater. Sci. Technol., 2*, 521-527 (1986). (Thermo; Theory)

86Zed: M.S. Zedalis and M.E. Fine, "Precipitation and Ostwald Ripening in Dilute Al-based-Zr-V Alloys," *Metall. Trans. A, 17*, 2187-2198 (1986). (Meta Phases; Crys Structure)

87Pan: S.K. Pandey, D.K. Gangopadhyay, and C. Suryanarayana, "Metastable Phases in Vapour-Deposited Al-Zr Thin Films," *Thin Solid Films, 146*, 273-282 (1987). (Meta Phases; Experimental)

87Reh: L.E. Reh, P.R. Okamoto, J. Pearson, R. Bhadra, and M. Grimsditch, "Solid-State Amorphization of Zr_3Al: Evidence of an Elastic Instability and First-Order Phase Transformation," *Phys. Rev. Lett., 59*(26), 2987-2990 (1987). (Meta Phases; Experimental)

87Vec: K.S. Vecchio and D.B. Williams, "Convergent Beam Electron Diffraction Study of Al_3Zr in Al-Zr and Al-Li-Zr Alloys," *Acta Metall., 35*(12), 2959-2970 (1987). (Meta Phases; Experimental)

88Boe: F. R. de Boer, R. Boom, W.C.M. Mattens, A.R. Miedema, and A.K. Niessen, *Cohesion in Metals*, North Holland, Amsterdam, 367 (1988). (Thermo; Theory)

88Cla: N.J. Clark and E. Wu, "Hydrogen Absorption by M_5X_3 Phase Zr-Al Compounds," *J. Less-Common Met., 142*, 145-154 (1988). (Meta Phases, Crys Structure; Experimental)

88Kim: S.J. Kim, R.J. Kematick, S.S. Yi, and H.F. Franzen, "On the Stabilization of Zr_5Al_3 in the Mn_5Si_3-Type Structure by Interstitial Oxygen," *J. Less-Common Met., 137*, 55-59 (1988). (Equi Diagram; Experimental)

88Sau: N. Saunders, Department of Materials Science and Engineering, University of Surrey, Internal Report INT-MSE-016 (1988). (Equi Diagram, Meta Phases, Thermo)

*Indicates key paper.
#Indicates presence of a phase diagram.

Al-Zr evaluation contributed by **J. Murray**, Alcoa Technical Center, Alloy Technical Division, Alcoa Center, PA 15069 and **A. Peruzzi** and **J.P. Abriata**, Centro Atómico Bariloche, Comisión Nacional de Energia Atómica, 8400 S.C. de Bariloche, Argentina. The work was supported by ASM International. Literature searched through 1988. Dr. Murray and Dr. Abriata are the Alloy Phase Diagram Program Category Editors for binary aluminum alloys and binary zirconium alloys, respectively.

The Li-N (Lithium-Nitrogen) System

By J. Sangster* and A.D. Pelton
Ecole Polytechnique de Montréal

Equilibrium Diagram

Figure 1 shows the assessed Li-N equilibrium diagram; Table 1 lists special points. Two known compounds in this system include Li_3N, which melts congruently, and LiN_3, which decomposes upon heating. The phase diagram has been studied only in the interval between Li and Li_3N. One eutectic invariant exists at 180.3 ± 0.1 °C. Figure 2 shows the detail of the eutectic region. Figure 3 shows the liquidus between 180 and 727 °C as a plot of $\log_{10}$(at.% N) vs reciprocal temperature.

The phase relations from 0 to 25 at.% N were determined by solubility [60Hof, 67Arn, 75Ada2, 75Yon] and thermal analysis [59Bol, 76Hub] techniques. A review of the earlier work was given by [75Ada1]. Experimental points from these studies are plotted in Fig. 1 to 3. Data of [59Bol], [67Arn], and [76Hub] were not tabulated by the authors; the data points shown in Fig. 1 to 3 were read from diagrams.

Table 2 summarizes the experimental conditions and methods. The solubility measurements of [75Yon] and [75Ada2], over the range from 200 to 450 °C, agree well, even though different experimental techniques were used both to add N and to measure the solubility limit at Li_3N saturation. Both studies began with Li of >99.9 wt.% purity, which was further purified with Zr, Y, or Ta getters. Least-squares fits in Fig. 3 to the data of [75Yon] or to the data of [75Ada2] gave nearly indistinguishable lines. The least-squares line shown in Fig. 3 was obtained from fitting the two sets of data:

$$\log_{10}(\text{at.\% N}) = 3.2455 - 2072/T \text{ (for } T < 723 \text{ K)} \qquad \text{(Eq 1)}$$

where T is in Kelvin.

Figure 3 shows that this line, when extrapolated to 727 °C, passes close to the experimental points of [59Bol]. These authors used a thermal analysis technique to measure the liquidus up to the melt-

*Permanent address: Sangster Research Laboratories, Suite 402, 3475 de la Montagne, Montréal Québec, Canada, H3G 2A4.

Table 1 Special Points of the Assessed Li-N Phase Diagram

Reaction	Compositions of the respective phases, at.% N			Temperature °C	Reaction type
$L \rightarrow \beta Li$		0		180.6	Melting
$\beta Li \rightarrow \alpha Li$		0		−193	Allotropic
$L \rightarrow (\beta Li) + Li_3N$	0.05	~0	25.0	180.3 ± 0.1	Eutectic
$L \rightarrow Li_3N$		25.0		813 ± 2	Congruent

Table 2 Experimental Conditions for Investigation of Li-Li_3N Phase Diagram

Temperature range, °C	Method of saturation	Determination of saturation point	Reference
180.2 to 180.5	Metered N_2 gas	Thermal analysis	[76Hub]
200 to 450	Metered N_2 gas	Measurement of electrical resistance	[75Ada2]
195 to 441	Excess Li_3N added	N analysis by Kjeldahl	[75Yon]
250 to 450	Excess Li_3N added	N analysis by Nessler reagent	[60Hof]
350 to 800	Excess Li_3N added	Thermal analysis	[59Bol]
250 to 318	Excess Li_3N added	Measurement of electrical resistance	[67Arn]